

## LONG *RXTE* OBSERVATIONS OF A2163

YOEL REPHAELI,<sup>1,2</sup> DUANE GRUBER,<sup>3</sup> AND YINON ARIELI<sup>2</sup>

*Received 2005 August 30; accepted 2006 May 10*

### ABSTRACT

A2163 was observed by the *RXTE* satellite for  $\sim 530$  ks during a 6 month period, starting in 2004 August. The cluster primary emission is from very hot intracluster gas with  $kT \sim 15$  keV, but this component does not by itself provide the best-fitting model. A secondary emission component is quite clearly needed, and while this could also be thermal at a temperature significantly lower than  $kT \sim 15$  keV, the best fit (to the combined PCA and HEXTE data sets) is obtained with a power-law secondary spectral component. The deduced parameters of the nonthermal (NT) emission imply a significant fractional flux amounting to  $\sim 25\%$  of the integrated 3–50 keV emission. NT emission is expected, given the intense level of radio emission, most prominently from a large extended (“halo”) central region of the cluster. Interpreting the deduced NT emission as Compton scattering of the radio-emitting relativistic electrons by the CMB, we estimate the volume-averaged value of the magnetic field in the extended radio region to be  $B \sim 0.4 \pm 0.2 \mu\text{G}$ .

*Subject headings:* galaxies: clusters: general — galaxies: clusters: individual (A2163) —  
 galaxies: magnetic fields — radiation mechanisms: nonthermal

*Online material:* color figure

### 1. INTRODUCTION

High-quality spatially resolved measurements with current X-ray satellites have clearly shown that intracluster (IC) gas is not isothermal. With increasing image detail, it will likely be found that nonisothermality is a general feature of clusters. This is only to be expected, given the gas extent, origin, and processes that have affected its evolution. The only justification for spectral fitting of the emission from a large cluster region by a single-temperature plasma-emission code (which has been a standard procedure) was insufficient spectral and spatial resolution.

Not only is the assumption of isothermality generally invalid when characterizing the emission from a large cluster region, but the expectation that the emission is *purely* thermal may also be doubtful when a wide spectral band is considered. This is particularly so in clusters with known extended regions of radio emission, where the radio-emitting relativistic electrons give rise to nonthermal (NT) X-ray emission by Compton scattering off the cosmic microwave background (CMB) radiation. The well-known possibility that cluster X-ray spectra may have high-energy power-law tails (e.g., Rephaeli 1977) has been largely ignored, also because of the low sensitivity of past X-ray satellites to the detection of the predicted low-level NT emission.

Nonisothermal gas distribution and NT emission are of considerable interest, both intrinsically, for the detailed understanding of the astrophysics of clusters, and in the use of cluster properties and phenomena as cosmological probes. X-ray emission is currently our best probe of the properties of IC gas; the thermal structure of the gas can yield important information on energy exchange and transport processes. More globally, detailed gas density and temperature profiles are required in the analysis of measurements of the Sunyaev-Zeldovich (S-Z) effect and its use as a cosmological probe of the global parameters of the universe and its large-scale structure. On the other hand, NT phenomena in clusters have the

potential to contribute significantly to our understanding of the origin of relativistic particles and magnetic fields. It is obvious, therefore, that there is strong motivation for a more realistic characterization of cluster X-ray spectra.

The search for NT X-ray emission in clusters has been advanced considerably by the *RXTE* and *BeppoSAX* satellites. We have initiated and analyzed long *RXTE* observations of the Coma cluster (Rephaeli et al. 1999; Rephaeli & Gruber 2002), A2319 (Gruber & Rephaeli 2002), and A2256 (Rephaeli & Gruber 2003). In all three clusters, we found evidence for a second spectral component. While a secondary emission component would generally reflect the nonisothermality of IC gas, we found that, in these three clusters, the additional emission is likely to be mostly NT in origin. In each of the clusters, this conclusion is based on the relative quality of the statistical fits (of thermal vs. NT models) and the high physical plausibility of NT X-ray emission in the central cluster region in which extended radio emission was measured. Similar *BeppoSAX* searches for NT in these and other clusters (including A119, A754, and A2199) also yielded evidence for NT emission in at least some of the clusters (Fusco-Femiano et al. 1999, 2000, 2003; Kaastra et al. 1999). Note that the significance of the *BeppoSAX* PDS results has been questioned by Rossetti & Molendi (2004), who claim that the level of instrumental error is higher than what was previously assumed, and that the detection of NT emission in Coma is much less significant than originally reported by Fusco-Femiano et al. (1999). However, this claim has been disputed by Fusco-Femiano et al. (2004).

The moderately distant cluster A2163,  $z = 0.203$ , is one of the hottest, most luminous clusters, and a prime target of radio, S-Z, and X-ray observations in recent years. Its extended central region of radio emission (Herbig & Birkinshaw 1994) was extensively mapped by Feretti et al. (2001); this radio halo is one of the largest and most luminous. Spatial correlation between bright regions in the *Chandra* and radio maps may be interpreted as evidence for intense merging activity (Markevitch & Vikhlinin 2001), which is thought to enhance the efficiency of particle acceleration. The gas temperature profile and a detailed temperature map were determined from *XMM-Newton* (Pratt et al. 2001) and *Chandra* (Govoni et al. 2004) measurements. Here we report the results from

<sup>1</sup> Center for Astrophysics and Space Sciences, University of California, San Diego, La Jolla, CA 92093-0424.

<sup>2</sup> School of Physics and Astronomy, Tel Aviv University, Tel Aviv, 69978, Israel.

<sup>3</sup> 4789 Panorama Drive, San Diego, CA 92116.

TABLE 1  
RESULTS OF THE SPECTRAL ANALYSIS

| Parameter   | Single R-S           | Two R-S              | R-S+Power Law                    |
|---|----------------------|----------------------|----------------------------------|
| $\chi^2/\text{dof}$ .....                             | 43.2/32              | 35.6/30              | 32.2/30                          |
| $kT_1$ (keV).....                                     | 15.5 [14.6, 16.4]    | 20.9 [15.6, 80]      | 14.5[12.1, 21.0]                 |
| Normalization <sup>a</sup> .....                      | 0.450 [0.043, 0.047] | 0.036 [0.001, 0.044] | 0.036 [0.022, 0.046]             |
| Fe abundance <sup>b</sup> .....                       | 0.24 [0.12, 0.37]    | 0.27 [0.12, 0.54]    | 0.32 [0.11, 0.79]                |
| $kT_2$ (keV).....                                     | ...                  | 5.7 [0.8, 14.3]      | ...                              |
| Normalization <sup>a</sup> .....                      | ...                  | 0.014 [0.001, 0.045] | 0.0035                           |
| $I_e$ (5 keV) ( $\text{cm}^{-2} \text{s}^{-1}$ )..... | ...                  | ...                  | $(1.33 \pm 0.45) \times 10^{-4}$ |
| Photon index .....                                    | ...                  | ...                  | 1.8 [−2.4, 2.7]                  |

NOTE.—All quoted errors are at the 90% confidence level.

<sup>a</sup> e.m. = Raymond-Smith emission measure in units of  $10^{-14} \int N_e N_H dV / 4\pi D^2$ , where  $D$  is the luminosity distance and  $N_e$  and  $N_H$  are the total number of electrons and protons, respectively.

<sup>b</sup> Abundance is expressed relative to solar values.

a very long observation of A2163, the most distant of the radio (halo) clusters, observed with the *RXTE*.

## 2. OBSERVATIONS AND DATA REDUCTION

A2163 observations, with the Proportional Counter Array (PCA) and the High Energy X-ray Timing Experiment (HEXTE) on *RXTE*, were made during 95 separate pointings in the period 2004 August 24–2005 March 11. Data from PCA detectors 0 and 2 were collected in the “Good Xenon” spectral mode, which produces a 256 channel count spectrum, nominally from 2 to 1000 keV. The background estimation tool was found to produce spectra with a several percent gain error for the epoch of these observations; this was corrected to better than 1% in the software. Data from the two independent HEXTE clusters of detectors were taken in event-by-event mode and were subsequently accumulated into 256 channel spectra, spanning 12–250 keV. To subtract the background, each HEXTE cluster was commanded to beam switch every 32 s between on-source and alternate off-source positions  $1.5^\circ$  on either side.

Standard screening criteria were applied to the data segments (Earth elevation angle, spacecraft pointing, avoidance of the South Atlantic Anomaly, times of geomagnetic activity), resulting in a net exposure time for PCA of 528 ks and an average exposure time of 212 ks for the HEXTE clusters. The HEXTE net observation times were shorter than the PCA time, because HEXTE spends half of the time measuring the background, and some more time is lost from electronic dead time caused by cosmic rays.

The PCA background was estimated with the L7/240 faint source model provided by the instrument team and was corrected for errors in detector gain independently in the two detectors. Uncertainties in the background correction precluded using PCA data above 17 keV. The total PCA counting rate was 8 counts  $\text{s}^{-1}$ , or 21% of background. For HEXTE, the net counting rate was 0.6 counts  $\text{s}^{-1}$ , or 0.4% of background. The PCA background level is estimated to be accurate within  $\sim 0.5\%$ , or 0.2 counts  $\text{s}^{-1}$ . The HEXTE background, which is directly measured, has been determined (MacDonald & Gruber 2000) to be accurate to within a few hundredths count  $\text{s}^{-1}$  in long exposures.

## 3. SPECTRAL ANALYSIS

Inspection of the screened light curves for PCA and HEXTE revealed no significant variation, as expected for a cluster of galaxies. Accordingly, we co-added all the selected PCA and HEXTE data to form net spectra for analysis. Spectra from the individual PCA detectors were also co-added, and the small differences in gain were accounted for in the generation of the energy-response matrices, following procedures prescribed by the PCA analysis team.

A small energy dependence for systematic errors (e.g., Gruber et al. 2001), averaging about 0.8%, was applied to the PCA spectrum. In addition, PCA spectral channels below 3 keV and above 17 keV were excluded because of sensitivity to artifacts in the background model, as well as the rapidly declining effective area of the PCA outside these bounds. On inspection of the high-energy channels of HEXTE, we restricted the analysis to data in the range 12–80 keV.

We fit the joint PCA and HEXTE spectra summed over all observations to three simple spectral models: a Raymond-Smith (R-S) thermal plasma emission model, two R-S models at different temperatures, and a R-S plus a power-law model. In addition, we have checked whether we can find a meaningful indication for a temperature structure by fitting the data with two R-S thermal components plus a power law. In all cases, most of the observed flux is in a primary  $\sim 15$  keV R-S component. Best-fit parameters and 90% confidence intervals are listed in Table 1. The best-fit temperature in the single isothermal gas model is  $15.5 \pm 0.9$  keV, in good agreement with the range determined from *XMM-Newton* (Pratt et al. 2001) and *Chandra* (Govoni et al. 2004). The observed  $\simeq 6.7$  keV Fe xxv  $K\alpha$  line yields an abundance of  $Z = 0.24 \pm 0.13 Z_\odot$  (where  $Z_\odot$  denotes solar abundance), quite consistent with previously determined values ( $\geq 0.2$ ). No cold absorption was measurable, and given the 3 keV PCA threshold, none was expected.

The fit to a single isothermal model is only marginally acceptable, with  $\chi^2 = 43.2$  for 32 degrees of freedom (dof). Residuals have a high-low-high pattern, which signals the need for another smooth spectral component. When a second thermal component is added, best-fit parameters are  $kT_1 \simeq 20.9$  keV and  $kT_2 \simeq 5.7$  keV, with the second component accounting for a minor fraction, roughly 1% of the 3–50 keV flux. For this fit,  $\chi^2 = 35.7$ , lower by 7.5 than the value obtained in the single R-S model. The  $F$ -test probability of the second component is 0.94 for 2 additional degrees of freedom. Although the  $\chi^2$  is acceptable for this fit, the 90% error bounds of [16, 80] keV for  $kT_1$  lie outside (in fact, well outside) the more tightly constrained values of  $11.5 \pm 1.5$  keV obtained with *ASCA* (Markevitch 1996),  $14.6 \pm 0.9$  keV with *Röntgensatellit* (*ROSAT*; Elbaz et al. 1995),  $14.6 \pm 0.5$  keV with *XMM-Newton* (Pratt et al. 2001), and  $12.4 \pm 0.7$  keV measured with *Chandra* (Govoni et al. 2004). We therefore view this solution as doubtful. Indeed, the range of solutions is very wide, because the problem is numerically highly degenerate. If we consider the possible sets of  $(kT_1, kT_2)$ , the value  $\chi^2 + 4.6$  defines the joint 90% probability contour in parameter space. The lowest temperature combination permitted in this range is  $kT_1 = 16.1$  keV and  $kT_2 = 0.8$  keV, with fractions of the 3–50 keV flux of 99% and 1%, respectively. The highest temperature combination has  $kT_1 \simeq 14.3$  keV and  $kT_2$  unbounded,

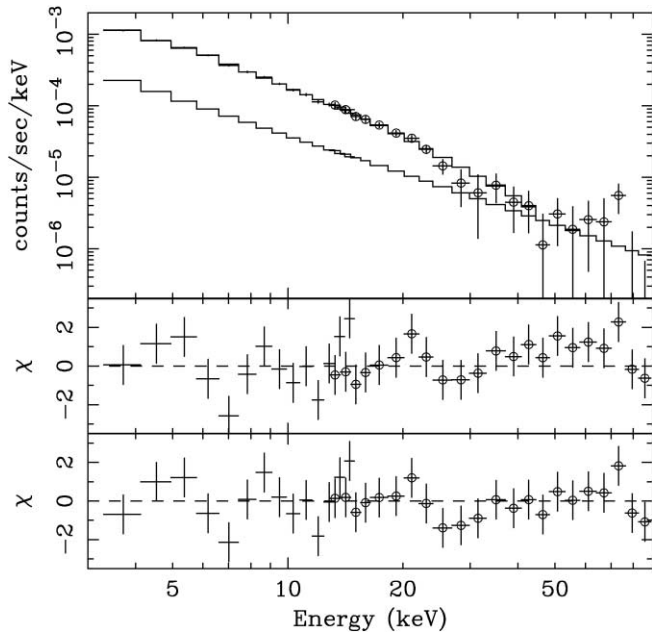


FIG. 1.—*RXTE* (photon) spectrum of A2163 and folded Raymond-Smith ( $kT_1 \simeq 14.5$  keV) and power-law (index  $\alpha = 1.8$ ) models. HEXTE data points are marked with circles and 68% error bars. The total fitted spectrum is shown with a histogram, while the lower histogram shows the power-law portion of the best fit. The quality of the fit is demonstrated in the lowest panel, which displays the observed difference normalized to the standard error of the data point. For comparison, the residuals of the fit to a single temperature model are shown in the middle panel. The improved quality of the fit to the combined thermal plus power-law components is apparent mostly at high energies. [See the electronic edition of the Journal for a color version of this figure.]

with 13% of the 3–50 keV flux in the higher temperature component. These results seem to indicate that the two-temperature fit improves on a single-temperature fit mostly by accounting for emission at the higher energy channels.

When the second component is a power law, the best fit has  $\chi^2 = 32.2$ , fully 11.0 lower than for the isothermal fit. The best-fit power-law index is  $\alpha = 1.8$ , with 90% confidence bounds of  $[-2.4, 2.7]$ , and the 3–80 keV flux is  $2.2 \times 10^{-11}$  ergs cm $^{-2}$  s $^{-1}$ , with 90% confidence bounds of  $[0.3, 4.1] \times 10^{-11}$  ergs cm $^{-2}$  s $^{-1}$ . The  $F$ -test probability of this power-law component is 0.99 for 2 additional degrees of freedom. The 3–50 keV flux of the power-law component is 27% of the total. This component comprises most of the flux at energies  $\geq 50$  keV. The iron abundance is  $Z = 0.32 Z_\odot$ , with 90% confidence bounds of  $[0.11, 0.79] Z_\odot$ . The best-fit fluxes from the combined thermal and power-law emissions, and that of just the power-law component, are shown in Figure 1, together with the data points. Residuals of this best-fit model are plotted in the lowest panel; for comparison, the residuals to the single-temperature model are shown in the middle panel. Differences between the latter two plots are apparent mostly at high energies.

The results of the temperature mapping with *XMM-Newton* (Pratt et al. 2001) and *Chandra* (Govoni et al. 2004) clearly necessitate inclusion of a temperature distribution in the fits. The *RXTE* field of view (FOV) includes a region that is much larger than that probed by both *XMM-Newton* and *Chandra*. This, and the fact that the *RXTE* lacks spatial resolution, make the *RXTE* insensitive to even large-scale features in the *Chandra* temperature map. The above fit to a two-temperature model grossly samples substantially different temperature components. Just to verify that we cannot get additional useful information from a more detailed spectral modeling, we have also considered a model with three components:

two R-Ss and a power law. When the model parameters are fully unconstrained, their values are obviously very loosely determined. The best fit to this model (with  $\chi^2 = 31.1$  for 28 dof) yields  $kT_1 = 16.3 \pm 1.2$  keV, a negligible second thermal component, with  $kT_2 = 3.7 \pm 7.5$  keV,  $Z = (0.28 \pm 0.16) Z_\odot$ ,  $\alpha = 1.3 \pm 3.0$ , and power-law normalization of  $(1.3 \pm 2.8) \times 10^{-11}$  ergs cm $^{-2}$  s $^{-1}$ . The decrease in  $\chi^2$  when a power-law component is added is 4.6, so (from  $F$ -test statistics) the significance is about 85% (or, more specifically, 83%–86%, depending on the particular choice of “interesting” parameters). However, the  $\chi^2$  hypersurface around the minimum corresponding to this parameter set is not very deep, meaning that a small increase of  $\chi^2$  above its minimum value results in a rather different parameter set. In spite of the implied substantial uncertainty, we find that the need for a power-law component is removed only when  $kT_1 \geq 30$  keV, which we consider to be rather unrealistic.

A power-law component at the above deduced level is apparent in the HEXTE measurements. To check general consistency between results from the PCA and HEXTE, we have determined the parameters of this component by analyzing HEXTE data separately. Clearly, due to the relatively high (12 keV) lowest energy channel of HEXTE, an appreciable fraction of the thermal emission cannot be detected by this experiment, so we have set the parameters of the isothermal component to its best-fit values from the joint (PCA + HEXTE) data. Fitting for the power law, we obtain  $\alpha \simeq 1.9^{+0.9}_{-0.6}$  and  $F(3 - 80 \text{ keV}) \simeq (2.5^{+1.2}_{-0.5}) \times 10^{-11}$  ergs cm $^{-2}$  s $^{-1}$  for the power-law (photon) index and the integrated 3–80 keV flux. Thus, HEXTE data alone provide significant additional evidence for NT emission, whose spectral index has a narrower 90% confidence interval than that determined in the joint fits. While this is a constrained fit, with only two free parameters, it is both physically (by virtue of the anticipated levels of thermal and NT emissions) and practically (given the relative insensitivity of HEXTE to emission at low energies) well motivated.

We note that a relatively short  $\sim 109$  ks observation of A2163 with *BeppoSAX* PDS yielded an upper limit on power-law emission,  $F(20 - 80 \text{ keV}) \leq 5.6 \times 10^{-12}$  ergs cm $^{-2}$  s $^{-1}$  (Feretti et al. 2001). Our much deeper observation yields a significant detection of NT emission with a flux level  $F(20 - 80 \text{ keV}) \simeq 1.1^{+1.7}_{-0.9} \times 10^{-11}$  ergs cm $^{-2}$  s $^{-1}$ , whose 90% confidence interval includes the PDS upper limit.

#### 4. DISCUSSION

The results of the above spectral analysis clearly indicate that the emission in A2163 cannot be described by a single-temperature emission model (as is apparent from positive residuals at both low and high energies). A better fit is provided by a two-temperature model, with the secondary thermal component accounting for the low-energy residuals. The *Chandra* temperature map of the central cluster region shows a region, roughly  $2' \times 2'$  in area, where the temperature is  $\sim 9$  keV. The secondary thermal component we deduce has a somewhat lower value, but given the large uncertainty in the value we deduce, the difference is not significant, as is the *rough* (i.e., due to the substantially larger [58' FWHM] *RXTE* FOV, which includes the emission from the cooler outer regions) consistency of the relative flux values of the two thermal components.

However, in the best-fitting model, the second component is not thermal, but rather a NT power law. Indeed, NT emission is expected from the populations of relativistic electrons that emit both the extended IC radio emission and the emission from the several powerful radio sources in the central  $\sim 2$  Mpc region of A2163. In Table 2, we list the measured radio fluxes and spectral (energy) indices for the dominant sources in the *RXTE* FOV. In

TABLE 2  
VALUES OF RADIO PARAMETERS (AND  $1\sigma$  ERRORS)

| Source              | Flux Density-20 cm<br>(mJy) | Spectral (Energy) Index | Size<br>(kpc) |
|---------------------|-----------------------------|-------------------------|---------------|
| Halo.....           | $155 \pm 2$                 | $1.6 \pm 0.3$           | $2070 \pm 70$ |
| Relic.....          | $18.7 \pm 0.3$              | $2.1 \pm 0.3$           | $460 \pm 40$  |
| J1615–062 (T1)..... | $34.5 \pm 0.5$              | $0.8 \pm 0.1$           | 450           |
| J1615–061 (T2)..... | $6.0 \pm 0.3$               | $0.8 \pm 0.1$           | 120           |
| J1616–062 (T3)..... | $24.9 \pm 0.4$              | $0.8 \pm 0.1$           | 270           |

NOTE.—Source size is based on a Hubble constant of  $70 \text{ km s}^{-1} \text{ Mpc}^{-1}$ .

addition to the remarkably luminous emission from the most extended, regularly shaped halo region, we include the emission from four sources measured by Feretti et al. (2001). Fluxes and spectral indices for the halo and “relic” sources are determined from VLA measurements at two frequencies in the 20 cm band. To estimate the expected X-ray fluxes, also from the three tailed (T) sources, we need to specify their spectral indices; since these were not given by Feretti et al. (2001), we adopt a typical value of  $0.8 \pm 0.1$ .

On the relevant spatial scales, the radiation field most tightly coupled to the electrons by Compton scattering is the CMB, coupling that is only further enhanced in A2163 ( $z = 0.203$ ), due to the  $(1+z)^4$  dependence of the CMB energy density. In order to quantify the emission that effectively results from the scattering, we need to determine the spectral density distribution of the electrons. Radio emission from the central extended source dominates the overall emission, and since we expect the mean, volume-averaged field in this extended source to be much lower than field strengths in the galactic radio sources, it is clear that most of the Compton-produced X-ray emission comes from the halo. Nonetheless, we have estimated the emission by relativistic electrons in the other sources listed in Table 2.

Compton fluxes of the radio sources in Table 2 can be estimated from their measured radio fluxes and estimated mean field values. The latter can be determined by assuming energy equipartition between particles and fields. This assumption may be roughly valid in the particles’ galactic sources, by virtue of the relatively short timescales of all the relevant processes governing the particles and fields: acceleration, couplings to the field, and interstellar gas. (We note in passing that the attainment of equipartition in the IC space is questionable. IC fields and particles are likely to be of galactic origin, but the evolution during their expulsion from galaxies and in IC space is quite different; effective equilibration is not likely to occur there.) Using the deduced values of the equipartition in the radio sources, we have estimated their respective Compton X-ray fluxes. These turn out to be quite small for the relic as well as the three tailed sources, whose combined flux in the 3–80 keV band is  $\leq 1\%$  of the measured value. Note that consideration of the dominant non-halo radio sources in the clusters in which we have previously found evidence for NT emission (Coma, A2256, and A2319) similarly shows that their predicted X-ray emission contributes negligibly to the deduced NT emission in each of these clusters.

Since the known radio sources in the central region of A2163 do not contribute appreciable X-ray emission, we attribute all the measured emission to electrons in the halo and proceed to determine the mean, volume-averaged field in this region,  $B_{\text{rx}}$ , using the Compton-synchrotron formulae (e.g., Rephaeli 1979). For consistency with the basic premise that most of the measured Compton flux is due to electrons in the halo, and the fact that the electron spectrum can be more precisely deduced from the radio data, we use the radio spectral index in order to infer the electron

index. Doing so, we compute  $B_{\text{rx}} \simeq 0.4 \pm 0.2 \mu\text{G}$ . It should be emphasized that the overall uncertainty in the estimated mean field is substantially higher than this formal error, due to the lack of spatial information on NT X-ray emission, which necessitates invoking the assumption that the emitting relativistic electrons and the field are cospatial.

As a consequence of the assumption that the spatial factors in the theoretical expressions for the radio and NT X-ray fluxes are roughly equal, it follows that the mean value of the deduced magnetic field is independent of the source size and distance. The relativistic electron energy density does depend on these parameters. Scaling to the observed radius of the diffuse radio emission and integrating the electron spectral distribution over all energies above 1 GeV, we obtain  $\rho_e \simeq 1.4^{+0.8}_{-0.7} \times 10^{-13} h_{70}^{-1} \text{ ergs cm}^{-3}$ , where  $h_{70}$  is the value of the Hubble constant in units of  $70 \text{ km s}^{-1} \text{ Mpc}^{-1}$ . Based on the high Galactic proton-to-electron energy density ratio of cosmic rays, it can be conjectured that the energetic proton energy density is much higher than this value. A more specific assessment cannot be made without consideration of the electron and proton origin and their respective energy losses.

IC magnetic fields can also be estimated from Faraday rotation measurements of background radio sources seen through clusters, yielding a different mean field value,  $B_{\text{fr}}$ . These measurements usually yield field values that are a few  $\mu\text{G}$  (see, e.g., Clarke et al. 2001, and the review by Carilli & Taylor 2002) up to an order of magnitude higher than the values of  $B_{\text{rx}}$ . Average field strength of a few  $\mu\text{G}$  over an extended cluster region would have important implications for the range of electron energies that are deduced from radio measurements, and therefore on the electron (synchrotron and Compton) energy-loss times. Weaker mean (volume-averaged) fields imply higher electron energies, and therefore shorter electron energy-loss times, with possibly important ramifications for relativistic electron models (e.g., Rephaeli 1979; Sarazin 1999; Ensslin et al. 1999; Brunetti et al. 2001; Petrosian 2001). However, the apparent discrepancy between deduced values of  $B_{\text{rx}}$  and  $B_{\text{fr}}$  is usually naively interpreted. In fact,  $B_{\text{rx}}$  and  $B_{\text{fr}}$  actually provide very different measures of the mean field strength:  $B_{\text{rx}}$  is essentially a weighted volume average of the relativistic electron density and of  $B^q$ , with  $q \geq 2$ , while  $B_{\text{fr}}$  is an average of the product of the line-of-sight component of the field and the gas density. In general, the overall spatial dependences of these averages are considerably different, and so are their deduced values. Specific examples and quantitative comparisons, including the impact of observational uncertainties, are given by Goldshmidt & Rephaeli (1993) and by Newman et al. (2002).

We are grateful to the referee for very helpful critical comments. This work was supported by a NASA grant at the University of California, San Diego.

## REFERENCES

- Brunetti, G., Setti, G., Feretti, L., & Giovannini, G. 2001, *MNRAS*, 320, 365  
Carilli, C. L., & Taylor, G. B. 2002, *ARA&A*, 40, 319  
Clarke, T. E., Kronberg, P. P., & Böhringer, H. 2001, *ApJ*, 547, L111  
Elbaz, D., Arnaud, M., & Böhringer, H. 1995, *A&A*, 293, 337  
Ensslin, T. A., et al. 1999, *A&A*, 344, 409  
Feretti, L., Fusco-Femiano, G., Giovannini, G., & Govoni, F. 2001, *A&A*, 373, 106  
Fusco-Femiano, R., et al. 1999, *ApJ*, 513, L21  
———. 2000, *ApJ*, 534, L7  
———. 2003, in *ASP Conf. Ser. 301, Matter and Energy in Clusters of Galaxies*, ed. S. Bowyer, & C.-Y. Hwang (San Francisco: ASP), 109  
———. 2004, *ApJ*, 602, L73  
Goldshmidt, O., & Rephaeli, Y. 1993, *ApJ*, 411, 518  
Govoni, F. et al. 2004, *ApJ*, 605, 695  
Gruber, D. E., & Rephaeli, Y. 2002, *ApJ*, 565, 877  
Gruber, D. E., et al. 2001, *ApJ*, 562, 499  
Herbig, T., & Birkinshaw, M. 1994, *BAAS*, 185, 5307  
Kaastra, J. S., et al. 1999, *ApJ*, 519, L119  
MacDonald, D., & Gruber, D. E. 2000, *BAAS*, 32, 1184  
Markevitch, M. 1996, *ApJ*, 465, L1  
Markevitch, M., & Vikhlinin, A. 2001, *ApJ*, 563, 95  
Newman, W. I., Newman, A. L., & Rephaeli, Y. 2002, *ApJ*, 575, 755  
Petrosian, V. 2001, *ApJ*, 557, 560  
Pratt, G. W., Arnaud, M., & Aghanim, N. 2001, in *Clusters of Galaxies and the High-Redshift Universe Observed in X-Rays XX1st Moriond Astrophysics Meeting*, ed. D. M. Neumann, & J. T. T. Van (Savoie: Les Arcs)  
Rephaeli, Y. 1977, *ApJ*, 212, 608  
———. 1979, *ApJ*, 227, 364  
Rephaeli, Y., & Gruber, D. E. 2002, *ApJ*, 579, 587  
———. 2003, *ApJ*, 595, 137  
Rephaeli, Y., Gruber, D. E., & Blanco, P. R. 1999, *ApJ*, 511, L21  
Rossetti, M., & Molendi, S. 2004, *A&A*, 414, L41  
Sarazin, C. L. 1999, *ApJ*, 520, 529